

Robust Kernel-based Feature Representation for 3D Point Cloud Analysis via Circular Graph Convolutional Network

Seung Hwan Jung, Yeong-Gil Shin, and Minyoung Chung*

Abstract—Feature descriptor of the point cloud is used in many applications such as registration and part segmentation from 3D point clouds. Discriminative representations of the local geometric features is unquestionably the most important task for accurate point cloud analyses. However, it is challenging to develop rotation or scale invariant descriptors. Most of the previous works have either ignored rotations or empirically studied optimal scale parameters, which hinder the applicability of the methods for real-world datasets. In this paper, we present a new local feature description method that is robust to rotation, density, and scales. Moreover, to improve representations of the local descriptors, we propose a global aggregation method. First, we place kernels aligned around each point regarding the normal direction. To avoid the sign problem of the normal vector, we use symmetric kernel point distribution regarding the tangent plane. From each kernel point, we first projected the points from the spatial space to the feature space, which is robust to multiscale and rotation, based on angles and distances. Subsequently, we perform graph convolutions by considering local kernel point structures and long-ranged global context, obtained by a global aggregation method. We experimented with our proposed descriptors on the benchmark datasets (i.e., ModelNet40 and ShapeNetPart) to evaluate the performance of registration, classification, and part segmentation on 3D point clouds. Our methods showed superior performances compared to the state-of-the-art methods by reducing 70% of the rotation and translation errors in the registration task. Our method also showed comparable performance in the classification and part segmentation tasks without any external data augmentations.

Index Terms—Angle-based kernel convolutions, global context aggregation, rotation robust point descriptor, scale adaptation, 3D point cloud analysis.

I. INTRODUCTION

PPOINT cloud analysis is becoming a popular research area since the 3D sensor has been growing its capability to capture rich geometric 3D information. The applications of point cloud analysis include, but are not restricted to, robotics, autonomous driving, and augmented/mixed reality. Extracting salient local geometric information is a fundamental task to analyze point clouds to either match correspondences between two objects [1] or analyzing the geometric information [2]. Recently, end-to-end learning based on point or graph convolutional networks is outperforming the earlier works, which were primarily developed on hand-crafted features descriptors [3] [4]. However, building rotation or scale invariant descriptor

is remaining as a difficult task in the field of computer vision research.

Descriptors for point cloud applications have been a wide research area for point cloud registration, model segmentation, and classification. PointNet [5] shows the new paradigm for point cloud analysis by introducing a permutation invariant method, however, it is difficult to encode the local geometric information. PPFNet [6] was presented to encode local features by employing PointNet [5] for local regions and DGCNN [2] encodes relative position of neighbors for each point. However, these methods are limited to extract rotation invariant features and highly dependent on the density of the input point cloud. In practice, note that the point cloud is irregularly distributed and not aligned to the same frame, indicating that dynamic density and random rotation of the input point cloud significantly affects the representation of the descriptors. KPConv [7] uses kernel points around each point to efficiently handle irregularly distributed point clouds. KPConv showed outperforming performance, nonetheless, rotation variant descriptor limits the performance on randomly rotated objects, which are obtained by multiview scans. 3DSmoothNet [1] extracts local region points and aligns the local points to the local reference frame of the center point. The main limitation of 3DSmoothNet is that a sign of a normal axis and directions of the other two axes is not unique in a planar region. Descriptors that are aligned by an inaccurate local reference frame may encode different geometric context. In the example of point cloud registration, if the corresponding points have different normal signs, descriptors from the points may hamper to find correspondences. Moreover, local descriptors only encode local geometric information, which is difficult to encode global geometry. Consequently, local descriptors on the monotonous and repeating area are typically considered as non-salient descriptors, which indicates that global registration can be mismatched.

To overcome the previous limitation, we propose a rotation robust and density robust descriptor generation method. Inspired by KPConv [7] and 3DSmoothNet [1], our proposed method aligns the kernels to the normal vector and extracts rotation robust features. Due to the nonuniqueness property of the local reference frame in the planar region, we distribute kernels in a form of the cylinder shape. This shape is symmetric regarding a tangent plane to handle the sign problem and has the circular cross-section to handle the other undefined reference axes. By employing this kernel structure, we apply convolution with adjacent kernels together in a way

Asterisk indicates corresponding author (chungmy@snu.ac.kr).

S. H. Jung, Y.-G. Shin, and *M. Chung are with the Department of Computer Science and Engineering, Seoul National University, Korea.

that the descriptor not to be affected by rotation. To make the descriptor robust to the scale of the local frame, we analyze the geometric information and rebuild the descriptor with modified kernel size. In addition, to improve representations of the descriptor from the monotonous and repeating area, we aggregate all features based on distances from each point to encode discriminative global features.

The major contributions of this work can be summarized as follows:

- Rotation robust descriptor is developed based on the kernel alignment.
- The sign problem, which is caused by the normal direction, is resolved by the proposed angle-based convolution.
- Scale factor, which is derived by the size of a kernel, is automatically defined for each point by the scale adaptation module.
- Global context is effectively extracted by the proposed aggregation method with each local context.

We experimented our proposed method on three kinds of tasks: registration, classification, and part segmentation. We trained and tested our proposed method on ModelNet40 [8] for classification and registration, and on ShapeNet [9] for segmentation.

The remainder of this paper is organized as follows. In Section II, several hand-crafted 3D features and deep learning-based 3D features are reviewed. The proposed method is described in Section III. The experimental results, discussion, and conclusion are presented in Sections IV, V, and VI, respectively.

II. RELATED WORKS

A. Hand-crafted 3D features

Before the advance of deep learning, 3D feature descriptor was developed based on the hand-crafting methods. Local descriptors were generated based on the relationship between a point and spatial neighborhoods around the point. In addition, some methods build rotation invariant descriptor based on a local reference frame. Spin Images [10] aligns neighbors using the surface normal of the interest point and represents aligned neighbors to cylindrical support region using radial and elevation coordinates. 3D Shape Context [11] represents neighbors in the support region with grid bins divided along the azimuth, elevation, and radial values. Unique Shape Context (USC) [12] extends the 3D Shape Context method by applying the local reference frame based on the covariance matrix. Similarly, Signature of Histograms of Orientations (SHOT) [3] also calculated the local reference frame and built a histogram using angles between point normal vectors. Point Feature Histograms (PFH) [13] and Fast Point Feature Histograms (FPFH) [4] selected neighbors for each point and built a histogram using pairwise geometric differences between neighbors and the interest point such as relative distance and angles. Recently, with the advent of deep neural networks for point cloud data (e.g., PointNet [5] and DGCNN [2]), the feature descriptors are showing groundbreaking results compared to the hand-crafted methods in many vision tasks.

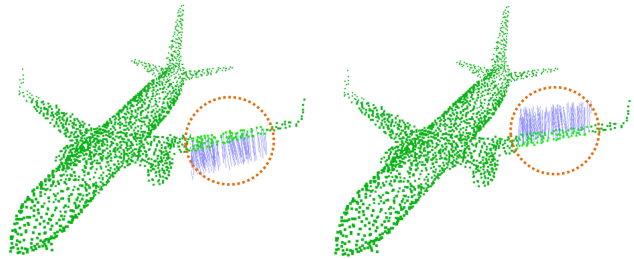


Fig. 1: Visualization of normal vectors. The signs for each point on a planar surface is not determined uniquely.

B. Deep learning based 3D features

1) *Volumetric based Methods*: Converting the point cloud to the volumetric data representation was widely used to employ grid-based convolutions [14], [15]. However, the quantification of the floating point data carried out an approximation, so that the input data intrinsically contains discretized artifacts. Since the voxelization process severely consumes the memory, these methods typically approximated the input data into a coarse grid of volumetric representation. To overcome this problem, some methods represented the point cloud data by optimizing memory consumption. OctNet [16] divided the space by employing a set of unbalanced octrees based on the density. Some methods used sparse tensor which only saves the non-empty space coordinates and features [17]–[19].

To build rotation invariant descriptor, 3DSmoothNet [1] calculated the local reference frame based on the covariance of points and transformed neighbor points within the spherical support area of the interest point using the local reference frame before voxelizing the points. However, a sign of a normal axis and directions of the other two axes is not unique in the planar region. Descriptors that are aligned using an inaccurate local reference frame may encode different geometric context. Therefore, we assume the sign of the normal vector is not unique and use a customized kernel similar to the KPConv [7] method to deal with the sign issue.

2) *Point based Methods*: PointNet [5] and PointNet++ [20] are the pioneer works for point cloud analysis, which are based on deep neural networks. These methods encode unstructured point clouds using a shared multilayer perceptron and build the permutation invariant descriptor using a global max-pooling layer. Based on PointNet, various methods have been developed to improve performance. PPFNet [6] extended PointNet [5] to learn local geometric features. PPFNet built local features by employing PointNet and subsequently fused global information based on the local features by employing max-pooling. PPF-FoldNet [21] used rotation invariant features such as angles and distances between the interest point and neighbor and trained the descriptor by using folding-based auto encoding within an unsupervised fashion. DGCNN [2] selected k-nearest neighbors for each point and encoded relative locations of the neighbors to encapsulate the geometric information. Kernel Point Convolution (KPConv) [7] proposed a kernel-based point convolution method which placed kernel

points around each point to effectively handle irregularly distributed point clouds, and further, aggregates the geometric information from the kernel points. We extended the KPConv method by employing normal based kernel alignment and angle-based convolution. As described in the KPConv, the normal vector is available for artificial data [7]. In the real-world dataset, a local reference frame is not accurate due to the sign problem (i.e., uncertain direction of normal vector; Fig. 1). To deal with the inaccurate local reference frame, we aligned the kernels and extracted features based on the unsigned normal axis, and subsequently applied convolution operation that are invariant to the sign problem.

III. METHOD

Figure 2 illustrates an overview of our proposed descriptor generation framework. The point descriptor is built by using information obtained from kernels around the point. To build rotation invariant kernels, we use normal vectors of each point to align the kernels (Section A). We extract local information from the kernels to encode feature descriptors (Section B). Subsequently, circular convolution is applied, which is invariant to the sign problem (Section C). The scale adaptation module is employed to the network to resolve scale issues (Section D). Various CNN encoder architectures are presented in Section E, which were used for downstream tasks in this study. Finally, the global context estimation is demonstrated that is employed to the encoder architectures (Section F).

A. Kernel alignment

To build a rotation robust descriptor, we align the kernels around each point using the local reference axis, i.e. normal vector. However, the sign of the normal vector and the remaining local reference axes are not unique if a point is located on a planar surface. To resolve the ambiguities, we use cylinder shape kernels, in which the cylinder column is aligned to the normal vector.

Figure 3(a) illustrates our kernel distribution. The cross-section of the cylinder is the circle along the normal direction. We place the kernels for each circle (i.e., four to six numbers of kernels), and group them as one layer. In total, we use three layers for the cylinder (i.e., additional upper and lower regions of the tangent plane).

B. Rotation robust feature projection

Once all the kernels are aligned for each point, we extract k -nearest neighbor points from each kernel. Averaged location is then calculated based on their distance from the kernel:

$$\hat{x}_i^k = \sum_{x_j \in N(x_i^k)} \frac{w_j x_j}{\sum w_j} \text{ where } w_j = \exp\left(\frac{-(x_j - x_i^k)^2}{d^2}\right), \quad (1)$$

where $\hat{x}_i^k \in \mathbb{R}^{N \times 3}$ is weighted averaged location of the k -th kernel point of x_i , and d indicates the distance from the center point to the kernel point. As a weighting term, i.e., w_j , we used the Gaussian function to reduce the influence of outliers in (1).

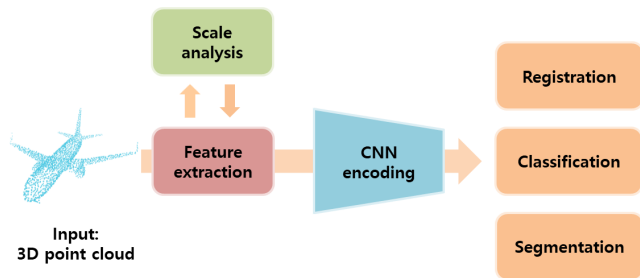


Fig. 2: Overview of the proposed architecture. First, we extract features using multiple kernel sizes. Subsequently, we employ scale analysis based on the interpolation between the kernel sizes. Finally, we encode the feature descriptor using the adjusted scale for the downstream tasks.

For rotation robust representations, we estimate four kinds of features. We first estimate angles between two vectors: one is from the center point of kernels to the weighted averaged point and the other is the normal vector (the angle $f1$ in Fig. 3(d)). However, since the normal vector has the normal orientation problem (i.e., sign ambiguity), we multiply negative sign to the normal vector if the kernel is located below the tangent plane:

$$f1_i^k = v_i \cdot \frac{\hat{x}_i^k - x_i}{\|\hat{x}_i^k - x_i\|} \cdot \text{sign}(k) \quad (2)$$

where v_i indicates the normal vector of x_i , and $\text{sign}(k)$ returns a negative sign if the kernel is located below the tangent plane. This term determines the angle value regardless of the normal sign.

Next, we estimate distances from the point to the averaged neighbors and from the center of the kernels to the averaged neighbors (the distances $f2$ and $f3$ in Fig. 3(d)):

$$f2_i^k = \left\| \frac{\hat{x}_i^k - x_i}{d} \right\| \quad (3)$$

$$f3_i^k = \left\| \frac{\hat{x}_i^k - x_i^k}{d} \right\| \quad (4)$$

To provide direction to the closest adjacent kernel points, we estimate the distance ratio from two adjacent kernel points to the averaged point (the ratio $f4$ in Fig. 3(d)):

$$f4_i^k = \frac{\|\hat{x}_i^k - x_i^{k+1}\|}{\|\hat{x}_i^k - x_i^{k+1}\| + \|\hat{x}_i^k - x_i^{k-1}\|} \quad (5)$$

The relative location of the averaged neighbor points can be successfully encoded based on the presented angle- and distance-based description. Figure 3 illustrates the entire process for the feature extraction process.

C. Circular convolution

Since the kernels are not aligned to the unique local reference frames, the order of the kernels may be changed depending on the point distribution. However, adjacent kernels within the cylinder layer are invariant to rotation. Therefore, we extend $1 \times 1 \times 1$ channel-wise convolution (6) to (7):

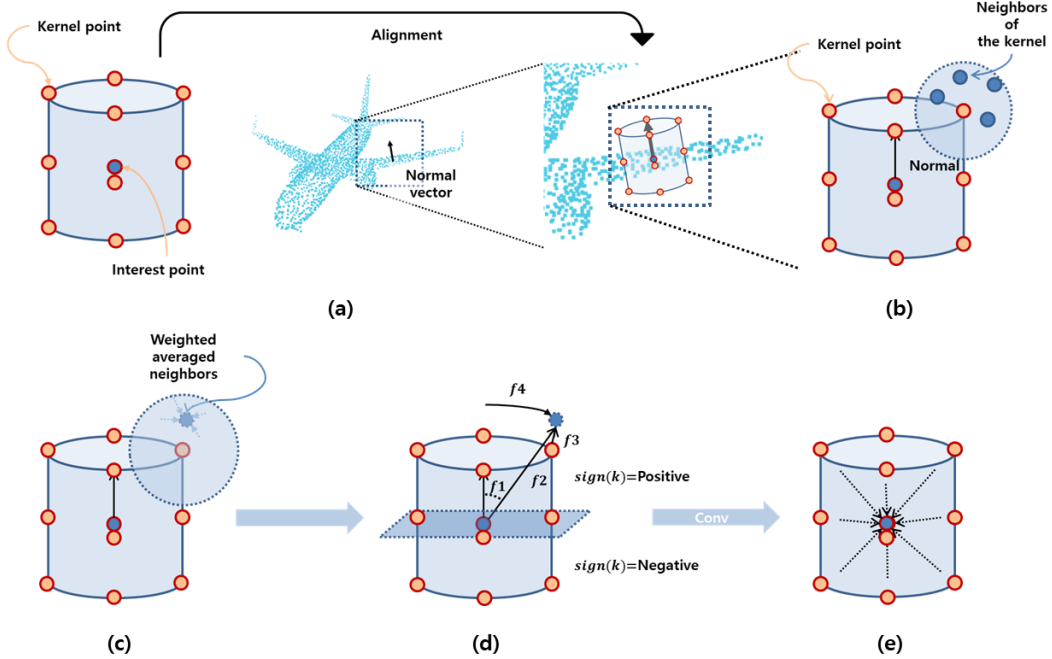


Fig. 3: (a) Kernel points are aligned using the normal vector of the target point. (b) Neighbors are selected for each kernel point. (c) Weighted averaged location is estimated based on the distance from the kernel point to the neighbors. (d) For each kernel, the relative location of the averaged neighbor is estimated using distances and angles. (e) After convolution, kernel features are aggregated by summation and maximum value selection to represent the interest point.

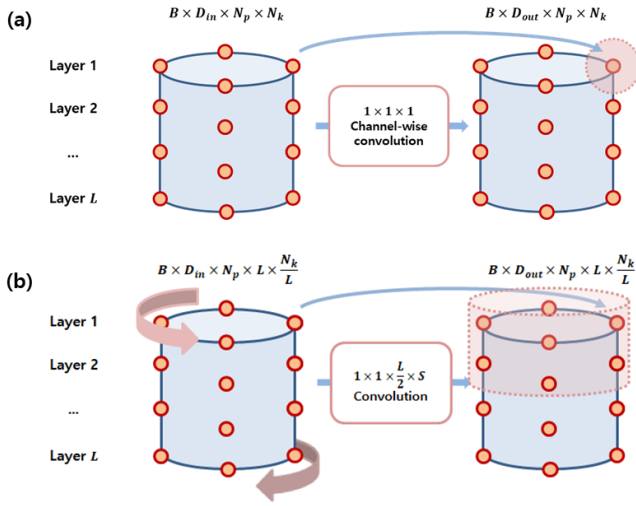


Fig. 4: (a) Channel-wise convolution and (b) circular convolution. The red transparent region indicates the receptive field. S indicates the kernel size of the convolution.

$$x_i = \sum_{\hat{x}_i^k} f(g(\hat{x}_i^k)), \quad (6)$$

$$x_i = \sum_{\hat{x}_i^k} f(g(\hat{x}_i^{c(k,-1)}), g(\hat{x}_i^k), g(\hat{x}_i^{c(k,+1)})), \quad (7)$$

where $c(k, +1)$ and $c(k, -1)$ indicate the clockwise and counterclockwise adjacent kernels of the k -th kernel in the cylinder layer. Subsequently, to avoid the sign problem, kernels are divided into two groups: one is the collection of kernels above the tangent plane and the other is the collection of kernels below the tangent plane. If the kernel belongs to the first group, we select the clockwise adjacent kernel in clockwise order. Otherwise, we select in counterclockwise order.

In addition, we process convolution with multiple layers if the layers belong to the same group, i.e., (7) is extended to

$$x_i = \sum_{\hat{x}_i^k} f(g(\hat{x}_i^k), g(\hat{x}_i^j)_{j \in adj(k)}), \quad (8)$$

where $adj(k)$ indicates a set of adjacent kernel points of the k -th kernel point in the same group. We used circular padding convolution operation to implement (8). Figure 4 illustrates the convolution process using kernels. After convolution, kernel features around the interest point are aggregated by summation and maximum value selection.

D. Scale adaptation module

To develop a scale-robust descriptor, we adjust the kernel size based on the analysis of the multiscaled features (d in (1)). We first extract multiple features using the multiple kernel sizes (feature extraction in Fig. 2). Subsequently, we concatenate the multiscaled features and estimate the interpolation weights between the kernel sizes. Simple convolution

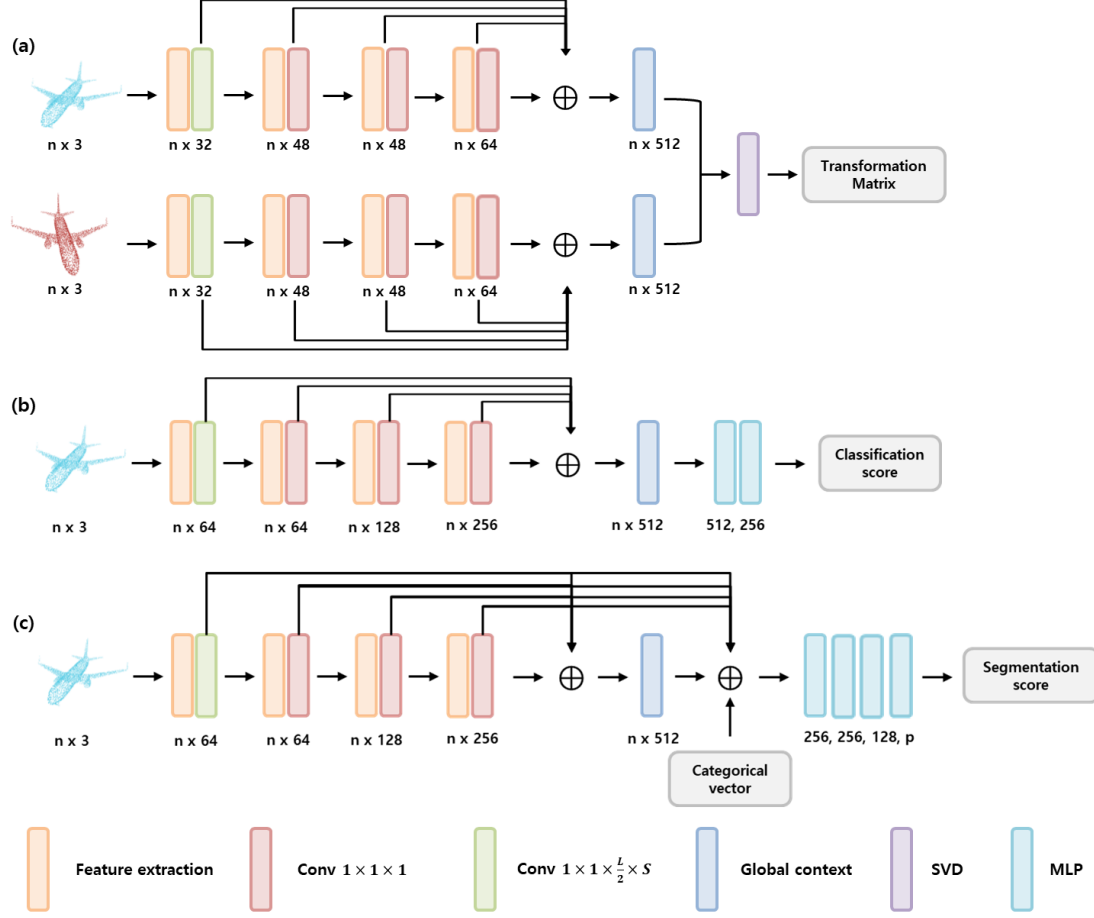


Fig. 5: Network architectures for (a) registration, (b) classification, and (c) part segmentation, respectively.

operations are employed for the scale analysis in Fig. 2. Finally, the output size of the kernel is used to encode the proposed descriptor for CNN encoding (Fig. 2).

E. CNN encoder architectures

The designed CNN encoders are illustrated in Figure 5. We first use four feature extraction layers. Using a shortcut connection, we concatenate multiscale features. Subsequently, global contexts from the concatenated features are estimated to improve representations (described in the following subsection, F). For the registration task, inspired by DCP [22], singular value decomposition (SVD) module is used to estimate the transformation matrix. For the classification and segmentation tasks, additional fully-connected layers (multi-layered perceptron; MLP) are used to estimate the scores. To demonstrate discriminative representations of our proposed method, we designed simple and low dimensional architectures to compared with the other methods.

F. Aggregating global context

Local descriptors on the monotonous and repeating area are typically considered as non-salient descriptors. To improve representations of the descriptor, we estimate global contexts

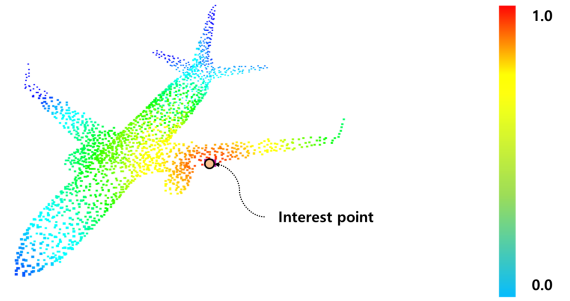


Fig. 6: Colors of point cloud indicate global context weights of the interest point. Red indicates a weight value of 1, and blue indicates a weight value of 0.

from local features (global context module in Fig. 5). Rather than estimating a single global context for all points by using max pooling, we estimate adaptive global contexts for each point by using distance-based weights.

To estimate the global feature for i th point, we calculate weights w_{ij} based on the gaussian distance between the i th and j th points (weights for an interest point in Fig. 6). Subsequently, averaged local features are estimated using the

Method	R-MSE	R-RMSE	R-MAE	T-MSE	T-RMSE	T-MAE	C
ICP	892.601135	29.876431	23.626110	0.086005	0.293266	0.251916	-
Go-ICP [23]	192.258636	13.865736	2.914169	0.000491	0.022154	0.006219	-
FGR [24]	97.002747	9.848997	1.445460	0.000182	0.013503	0.002231	-
PointNetLK [25]	306.323975	17.502113	5.280545	0.000784	0.028007	0.007203	20
PointNetLK [25]	227.870331	15.095374	4.225304	0.000487	0.022065	0.005404	40
DCP-v2 [22]	9.923701	3.150190	2.007210	0.000025	0.005039	0.003703	20
DCP-v2 [22]	1.307329	1.143385	0.770573	0.000003	0.001786	0.001195	40
Our method	0.017159	0.130991	0.064475	0.000000	0.000048	0.000027	20

TABLE I: ModelNet40 registration results. Evaluation metrics are mean squared error (MSE), root mean squared error (RMSE), and mean absolute error (MAE) for rotation (R-) and translation (T-). C indicates the number of categories for training.

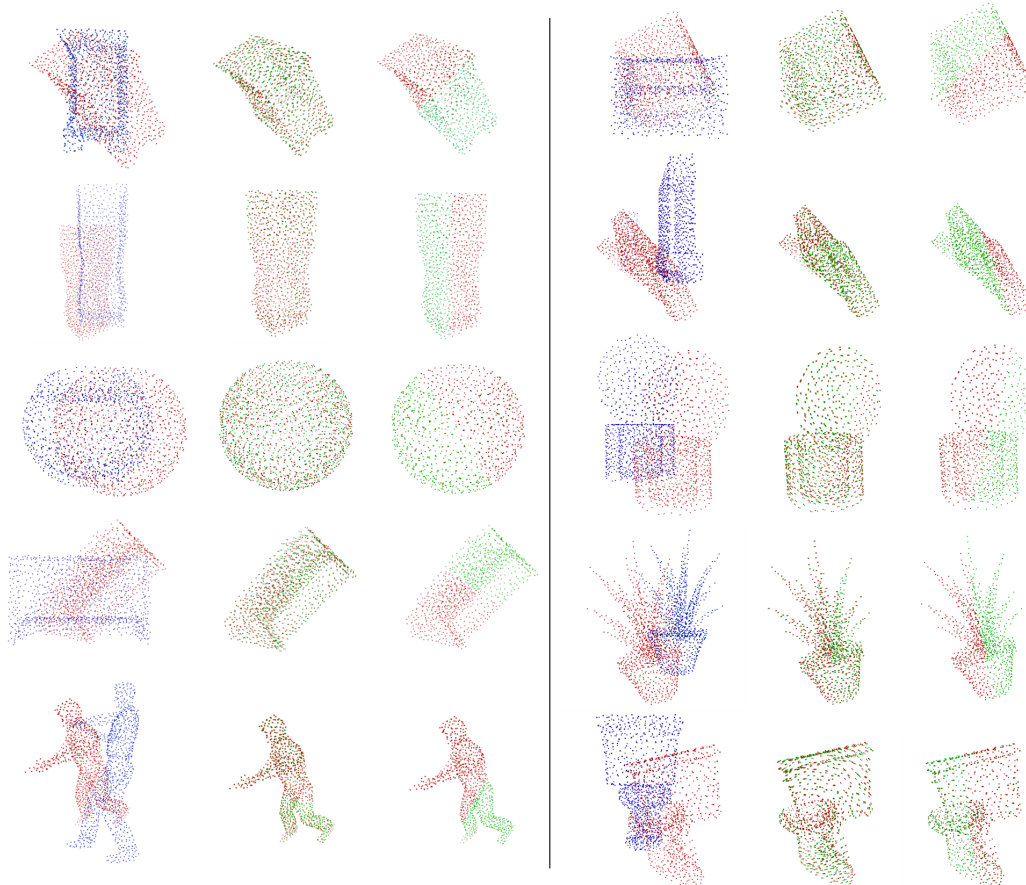


Fig. 7: Left: source (blue) and target (red) point clouds, Middle: registration results of DCP [22]. Green indicates the transformed source point clouds. Right: registration results of our method.

weights w_{ij} for all j .

$$g_i = \sum \frac{w_{ij} f_j}{\sum w_{ij}} \text{ where } w_{ij} = \exp\left(\frac{-(x_j - x_i)^2}{d^2}\right) \quad (9)$$

Once the global contexts are estimated for each point, we concatenate the global contexts to each local feature. Lastly, we perform convolution operation to the concatenated features.

IV. RESULT

We implement three tasks, registration, classification and segmentation. For registration and classification tasks, we use the ModelNet40 database [8]. For segmentation task, we used the ShapenetPart [9] database. For registration task, we

compared our methods to PointNetLK [25], DCP [22]. In case of classification and part segmentation tasks, we compared to the several methods such as PointNet [5], DGCNN [2], and KPConv [7].

A. Registration

We experimented our method on the ModelNet40 registration [8]. ModelNet40 contains 12,311 meshed CAD models from 40 categories. ModelNet40 is split by category into training and test sets: the first 20 categories among the 40 categories are used for training. For each model, we use 1,024 points for training and testing.

Method	OA	mIoU
SPLATNet [26]	-	85.4
SGPN [27]	-	85.8
3DmFV-Net [28]	91.6	84.3
SynSpecCNN [29]	-	84.7
RSNet [30]	-	84.9
SpecGCN [31]	91.5	85.4
PointNet [5]	89.2	83.7
PointNet++ [20]	90.7	85.1
KD-Net [32]	90.6	82.3
SO-Net [33]	90.9	84.9
PCNN by Ext [34]	92.3	85.1
SpiderCNN [35]	90.5	85.3
MCCConv [36]	90.9	85.9
FlexConv [37]	90.2	85.0
PointCNN [38]	92.2	86.1
DGCNN [2]	92.2	84.7
SubSparseCNN [28]	-	86.0
KPConv [7]	92.9	86.2
Our method	92.2	84.5

TABLE II: ModelNet40 classification results and ShapeNet-Part segmentation results

DCP [22] presented the end-to-end network for rigid registration. Inspired by the method, we use the SVD module to compute a rigid transformation. Figure 5 (a) illustrates the registration architecture. As evaluation metrics, mean squared error (MSE), root mean squared error (RMSE), and mean absolute error (MAE) are used for rotation and translation.

As listed in Table I, our method significantly reduced the registration errors compared to the other methods. Even when compared to the results trained with all categories, our method showed better performance. Figure 7 illustrates the registration results of DCP [22] and our method. Results of DCP [22] showed a small error between the two point clouds. On the contrary, the results of our method showed superior performance on matching. These results indicate that the proposed descriptor has better matched the feature-based correspondences between the source and target points, compared to the DCP [22].

B. Classification and Segmentation

We experimented our method on ModelNet40 [8] for classification and ShapenetPart [9] for part segmentation. ModelNet40 contains 12,311 models. Among the models, 9,843 models are used for training and the remaining 2,468 models are used for testing. For each model, we use 1,024 points for training and testing. ShapenetPart contains 16,681 models from 16 categories. Each point is annotated with part labels. For each model, we use 2,048 points for training and testing.

Figure 5 (b) and (c) illustrates the classification and part segmentation architectures. Table II lists the classification and part segmentation results. As for the evaluation metrics, overall accuracy (OA) is used for Modelnet40 classification and instance average IoU (mIoU) is used for ShapeNetPart segmentation. As clearly demonstrated in Table II, our proposed descriptor achieved a comparable performance compared to the state-of-arts. Figure 8 illustrates the example outputs of the proposed method.

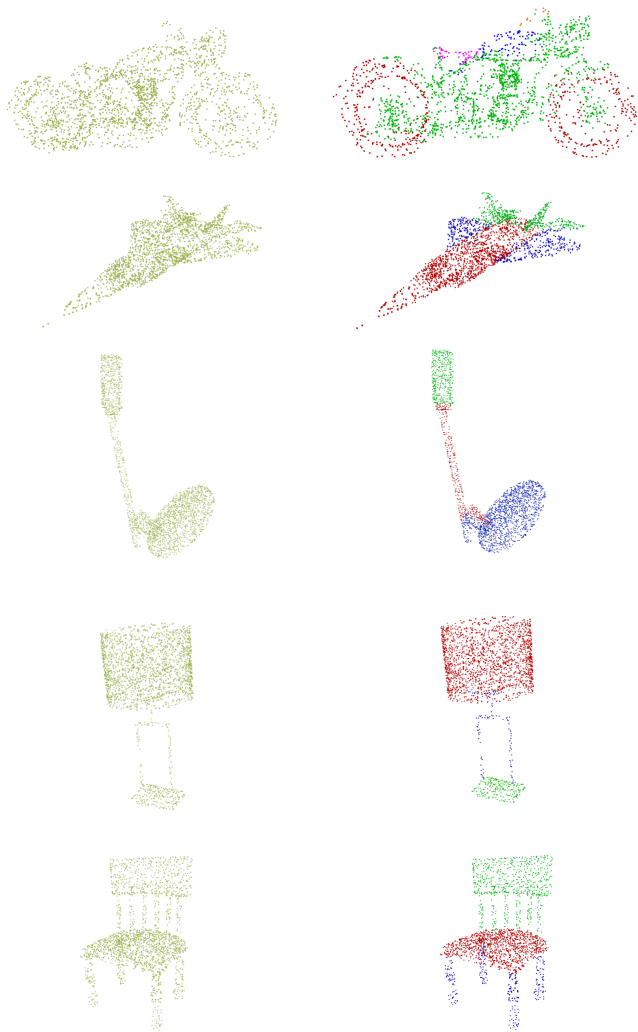


Fig. 8: Left: source points. Right: part segmentation results

C. Parameter and ablation study

We conduct several parameter and ablation studies on the registration task to verify the effect of our method (Table III): convolution operation, the number of nearest neighbors for each kernel, scale adaptation module, and global context.

First, we experiment with the convolution methods: $1 \times 1 \times 1$ channel-wise convolution and circular convolution method. The network with the circular convolution significantly improved the performance regarding both rotation and translation. These results indicate that the circular convolution operations successfully captured the geometric features based on adjacent kernels. Figure 9 illustrates the registration results according to the kernel alignment and convolution methods. As illustrated, the network with the aligned kernel-based circular convolution showed better registration results.

Second, we experimented our method with a different number of neighbors. As listed in Table III, the errors are not significantly dependent on the number of neighbors. Since we used the distance-based weights for each neighbor, the closer neighbors have more influences. By using the distance-based weights, employing the averaged neighbors reduced the

Conv method	R-MSE	R-RMSE	R-MAE	T-MSE	T-RMSE	T-MAE
channel-wise	0.040420	0.201046	0.105576	0.000000	0.000149	0.000094
circular conv	0.017159	0.130991	0.064475	0.000000	0.000048	0.000027
KNN	R-MSE	R-RMSE	R-MAE	T-MSE	T-RMSE	T-MAE
10	0.017159	0.130991	0.064475	0.000000	0.000048	0.000027
2	0.014517	0.120486	0.065029	0.000000	0.000037	0.000025
Global information	R-MSE	R-RMSE	R-MAE	T-MSE	T-RMSE	T-MAE
X	0.017159	0.130991	0.064475	0.000000	0.000048	0.000027
O	0.008142	0.091766	0.046526	0.000000	0.000047	0.000027
Scale adaptation	R-MSE	R-RMSE	R-MAE	T-MSE	T-RMSE	T-MAE
X	0.017159	0.130991	0.064475	0.000000	0.000048	0.000027
O	0.021910	0.148021	0.055841	0.000000	0.000039	0.000025

TABLE III: Parameter and ablation study

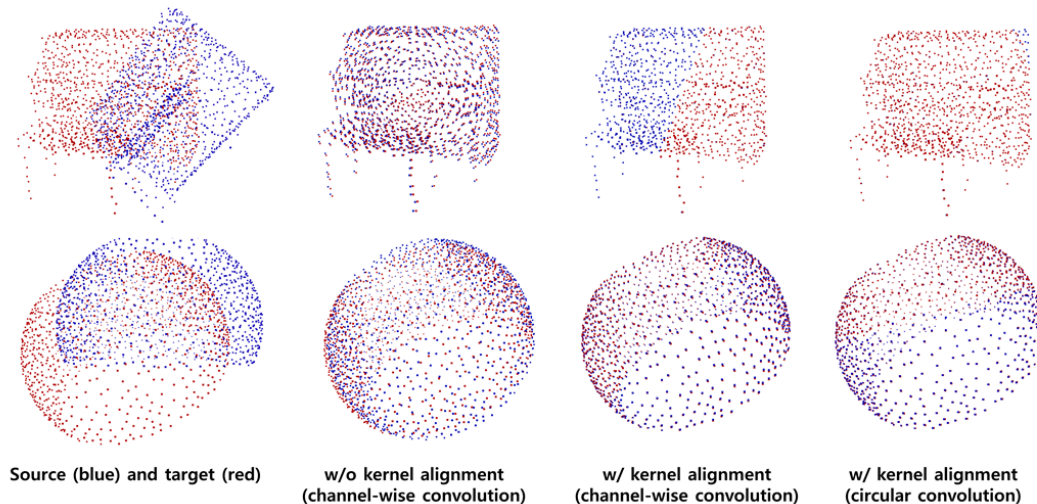


Fig. 9: Comparison of methods

influence from the number of neighbors.

Third, we conducted the registration with the global context. As a result, the rotation error is decreased largely compared to the other experiments. These results demonstrate that the global context resolves the ambiguities for each local descriptor.

Lastly, we experimented the scale adaptation module. We fed multiple kernel sizes into the proposed scale adaptation module. The network with the scale adaptation module showed comparable performance with the network with heuristically selected kernel sizes. The results indicate that the scale adaptation module found the optimal kernel size to capture the geometric information.

V. DISCUSSION

Point cloud analysis requires a rotation, density, and scale robust feature representation. It is challenging to obtain the presented robustness at the same time because there is a trade-off between the rotation and density robustness. In this study, we propose an aligned kernel-based feature representation to resolve the limitations. Our method is based on the kernels inspired by the KPConv to obtain density robust characteristics. To make the descriptor robust to rotation, we align kernels to the local reference frame. Subsequently, we apply normal sign independent convolutions to the descriptors rather

than using fixed kernels independent to rotations [7]. Instead of using translation invariant features [2], we used rotation robust features from aligned kernels. In addition, to improve representations of the descriptor, we estimate adaptive global context for each point rather than using a single global context [6]. Since the kernel-based descriptors are highly dependent on the size of the given kernels, we adjusted the kernel size based on the trainable weights.

The experimental results for various tasks (i.e., registration, classification, and part segmentation) showed promising results for feature representation. In the registration task, the rotation and translation errors have decreased significantly. This indicates that our descriptors successfully capture salient and corresponding geometric information between the two transformed point clouds. In the case of classification and segmentation tasks, our proposed method showed comparable performance with simple and low dimensional architectures. These results indicate that our method is not only limited to the transformed point cloud task but also applicable to the general purpose (i.e., feature representations). Several parameter and ablation studies have also demonstrated that our proposed methods improved the feature representations and stability of the descriptor.

VI. CONCLUSION

Encoding a rotation, density, and scale robust feature is a challenging task for point cloud representation. One for each robustness is critical for successful application in various downstream tasks. In this paper, we proposed a CNN-based feature encoding method to resolve the task. The proposed kernel alignment, feature projection, and kernel conscious graph convolution methods have demonstrated superior performance on the registration task compared to any other previous methods. Moreover, the proposed scale adaptation and global aggregation methods have successfully captured the optimum scale parameter and global geometric features for each local descriptors, respectively.

REFERENCES

- [1] Z. Gojcic, C. Zhou, J. D. Wegner, and A. Wieser, "The perfect match: 3d point cloud matching with smoothed densities," in *2019 IEEE/CVF Conference on Computer Vision and Pattern Recognition (CVPR)*, 2019, pp. 5540–5549.
- [2] A. V. Phan, M. L. Nguyen, Y. L. H. Nguyen, and L. T. Bui, "Dgcnn: A convolutional neural network over large-scale labeled graphs," *Neural Networks*, vol. 108, pp. 533 – 543, 2018. [Online]. Available: <http://www.sciencedirect.com/science/article/pii/S0893608018302636>
- [3] S. Salti, F. Tombari, and L. Di Stefano, "Shot: Unique signatures of histograms for surface and texture description," *Computer Vision and Image Understanding*, vol. 125, 08 2014.
- [4] R. B. Rusu, N. Blodow, and M. Beetz, "Fast point feature histograms (fpfh) for 3d registration," in *2009 IEEE International Conference on Robotics and Automation*, 2009, pp. 3212–3217.
- [5] R. Q. Charles, H. Su, M. Kaichun, and L. J. Guibas, "Pointnet: Deep learning on point sets for 3d classification and segmentation," in *2017 IEEE Conference on Computer Vision and Pattern Recognition (CVPR)*, 2017, pp. 77–85.
- [6] H. Deng, T. Birdal, and S. Ilic, "Ppfnet: Global context aware local features for robust 3d point matching," in *2018 IEEE/CVF Conference on Computer Vision and Pattern Recognition*, 2018, pp. 195–205.
- [7] H. Thomas, C. R. Qi, J. Deschaud, B. Marcotegui, F. Goulette, and L. Guibas, "Kpconv: Flexible and deformable convolution for point clouds," in *2019 IEEE/CVF International Conference on Computer Vision (ICCV)*, 2019, pp. 6410–6419.
- [8] Zhirong Wu, S. Song, A. Khosla, Fisher Yu, Linguang Zhang, Xiaoou Tang, and J. Xiao, "3d shapenets: A deep representation for volumetric shapes," in *2015 IEEE Conference on Computer Vision and Pattern Recognition (CVPR)*, 2015, pp. 1912–1920.
- [9] L. Yi, V. G. Kim, D. Ceylan, I. Shen, M. Yan, H. Su, C. Lu, Q. Huang, A. Sheffer, and L. Guibas, "A scalable active framework for region annotation in 3d shape collections," *ACM Transactions on Graphics (TOG)*, vol. 35, pp. 1 – 12, 2016.
- [10] A. E. Johnson and M. Hebert, "Using spin images for efficient object recognition in cluttered 3d scenes," *IEEE Transactions on Pattern Analysis and Machine Intelligence*, vol. 21, no. 5, pp. 433–449, 1999.
- [11] A. Frome, D. Huber, R. Kolluri, T. Bülow, and J. Malik, "Recognizing objects in range data using regional point descriptors," vol. 3, 05 2004, pp. 224–237.
- [12] F. Tombari, S. Salti, and L. Di Stefano, "Unique shape context for 3d data description," 01 2010.
- [13] R. Rusu, N. Blodow, Z. Marton, and M. Beetz, "Aligning point cloud views using persistent feature histograms," 09 2008, pp. 3384–3391.
- [14] D. Maturana and S. Scherer, "Voxnet: A 3d convolutional neural network for real-time object recognition," in *2015 IEEE/RSJ International Conference on Intelligent Robots and Systems (IROS)*, 2015, pp. 922–928.
- [15] C. Ruizhongtai Qi, H. Su, M. NieBner, A. Dai, M. Yan, and L. Guibas, "Volumetric and multi-view cnns for object classification on 3d data," 06 2016, pp. 5648–5656.
- [16] G. Riegler, A. O. Ulusoy, and A. Geiger, "Octnet: Learning deep 3d representations at high resolutions," in *2017 IEEE Conference on Computer Vision and Pattern Recognition (CVPR)*, 2017, pp. 6620–6629.
- [17] B. Graham, "Spatially-sparse convolutional neural networks," 2014.
- [18] C. Choy, J. Gwak, and S. Savarese, "4d spatio-temporal convnets: Minkowski convolutional neural networks," 06 2019, pp. 3070–3079.
- [19] C. Choy, J. Park, and V. Koltun, "Fully convolutional geometric features," in *2019 IEEE/CVF International Conference on Computer Vision (ICCV)*, 2019, pp. 8957–8965.
- [20] C. R. Qi, L. Yi, H. Su, and L. J. Guibas, "Pointnet++: Deep hierarchical feature learning on point sets in a metric space," in *Advances in Neural Information Processing Systems 30: Annual Conference on Neural Information Processing Systems 2017, 4-9 December 2017, Long Beach, CA, USA*, I. Guyon, U. von Luxburg, S. Bengio, H. M. Wallach, R. Fergus, S. V. N. Vishwanathan, and R. Garnett, Eds., 2017, pp. 5099–5108. [Online]. Available: <http://papers.nips.cc/paper/7095-pointnet-deep-hierarchical-feature-learning-on-point-sets-in-a-metric-space>
- [21] H. Deng, T. Birdal, and S. Ilic, "Ppf-foldnet: Unsupervised learning of rotation invariant 3d local descriptors," in *ECCV*, 2018.
- [22] Y. Wang and J. Solomon, "Deep closest point: Learning representations for point cloud registration," 10 2019, pp. 3522–3531.
- [23] J. Yang, H. Li, D. Campbell, and Y. Jia, "Go-icp: A globally optimal solution to 3d icp point-set registration," *IEEE Transactions on Pattern Analysis and Machine Intelligence*, vol. 38, no. 11, pp. 2241–2254, 2016.
- [24] Q.-Y. Zhou, J. Park, and V. Koltun, *Fast Global Registration*, 2016, pp. 766–782. [Online]. Available: <https://app.dimensions.ai/details/publication/pub.1034541096>
- [25] Y. Aoki, H. Goforth, R. A. Srivatsan, and S. Lucey, "Pointnetlk: Robust efficient point cloud registration using pointnet," in *2019 IEEE/CVF Conference on Computer Vision and Pattern Recognition (CVPR)*, 2019, pp. 7156–7165.
- [26] H. Su, V. Jampani, D. Sun, S. Maji, E. Kalogerakis, M.-H. Yang, and J. Kautz, "Splatnet: Sparse lattice networks for point cloud processing," 06 2018, pp. 2530–2539.
- [27] W. Wang, R. Yu, Q. Huang, and U. Neumann, "Sgpn: Similarity group proposal network for 3d point cloud instance segmentation," in *2018 IEEE/CVF Conference on Computer Vision and Pattern Recognition*, 2018, pp. 2569–2578.
- [28] B. Graham, M. Engelcke, and L. v. d. Maaten, "3d semantic segmentation with submanifold sparse convolutional networks," in *2018 IEEE/CVF Conference on Computer Vision and Pattern Recognition*, 2018, pp. 9224–9232.
- [29] L. Yi, H. Su, X. Guo, and L. Guibas, "Syncspecnn: Synchronized spectral cnn for 3d shape segmentation," in *2017 IEEE Conference on Computer Vision and Pattern Recognition (CVPR)*, 2017, pp. 6584–6592.
- [30] Q. Huang, W. Wang, and U. Neumann, "Recurrent slice networks for 3d segmentation of point clouds," in *2018 IEEE/CVF Conference on Computer Vision and Pattern Recognition*, 2018, pp. 2626–2635.
- [31] C. Wang, B. Samari, and K. Siddiqi, *Local Spectral Graph Convolution for Point Set Feature Learning: 15th European Conference, Munich, Germany, September 8-14, 2018, Proceedings, Part IV*, 09 2018, pp. 56–71.
- [32] R. Klovov and V. Lempitsky, "Escape from cells: Deep kd-networks for the recognition of 3d point cloud models," in *2017 IEEE International Conference on Computer Vision (ICCV)*, 2017, pp. 863–872.
- [33] J. Li, B. M. Chen, and G. H. Lee, "So-net: Self-organizing network for point cloud analysis," in *2018 IEEE/CVF Conference on Computer Vision and Pattern Recognition*, 2018, pp. 9397–9406.
- [34] M. Atzmon, H. Maron, and Y. Lipman, "Point convolutional neural networks by extension operators," *ACM Trans. Graph.*, vol. 37, no. 4, Jul. 2018. [Online]. Available: <https://doi.org/10.1145/3197517.3201301>
- [35] Y. Xu, T. Fan, M. Xu, L. Zeng, and Y. Qiao, "Spidercnn: Deep learning on point sets with parameterized convolutional filters," 03 2018.
- [36] P. Hermosilla, T. Ritschel, P.-P. Vazquez Alcocer, A. Vinacua, and T. Ropinski, "Monte carlo convolution for learning on non-uniformly sampled point clouds," vol. 37, 12 2018, pp. 1–12.
- [37] F. Groh, P. Wieschollek, and H. Lensch, *Flex-Convolution: Million-Scale Point-Cloud Learning Beyond Grid-Worlds*, 05 2019, pp. 105–122.
- [38] Y. Li, R. Bu, M. Sun, W. Wu, X. Di, and B. Chen, "Pointcnn: Convolution on x-transformed points," in *NeurIPS*, 2018.